BUTTERWORTH HEINEMANN

Polymer Vol. 36 No. 11, pp. 2197–2201, 1995

0032-3861/95/$10.00 + 0.00

Two-phase structure and mechanical properties of poly(methyl methacrylate)/poly(ethylene-*co*-vinylacetate) alloys by polymerization-induced phase decomposition

Takayuki Kojima, Takashi Ohnaga* and Takashi Inoue†
Department of Organic and Polymeric Materials, Tokyo Institute of Technology, Ookayama, Meguro-ku, Tokyo 152, Japan
(Received 16 May 1994; revised 31 October 1994)

A binary alloy of poly(methyl methacrylate) (PMMA) and poly(ethylene-*co*-vinylacetate) (EVA) prepared by polymerization-induced phase decomposition had a two-phase structure, in which PMMA particles with uniform size were regularly dispersed in an EVA matrix, even when EVA was the minor component (e.g. 20%). This alloy exhibited high impact strength, high heat resistance and a high Young's modulus close to that of PMMA. To understand the morphology–properties relationship, we undertook a two-dimensional finite element method analysis of the deformation mechanism. A two-phase model was constructed so that four particles of PMMA were embedded in the EVA matrix. When the volume fraction of PMMA was close to 1, the model behaved as a rigid and deformable material even though PMMA was the dispersed phase. The rigid character seems to be caused by a stress concentration on the PMMA particles which are forced to dilate, especially when the particle-to-particle ligament thickness is small. The high impact strength was also interpreted in terms of the stress concentration on PMMA particles; i.e. the brittle PMMA can undergo plastic deformation induced by the large compressive stress evolved by bulk deformation, so that the impact energy is absorbed by the plastic deformation.

(Keywords: PMMA/EVA alloy; structure–properties relationship; finite element method)

INTRODUCTION

Rubber-toughened plastics, such as high impact polystyrene (HIPS) and acrylonitrile–butadiene–styrene (ABS) resin, constitute an important class of commercial thermoplastics[1]. HIPS is produced by the polymerization of a homogeneous solution of styrene and polybutadiene. It is well known that the multiphase structure is formed by phase separation induced by polymerization. Since the properties of HIPS depend on its structure, much effort has been directed towards controlling the structure. The mechanism of structure formation could be understood in terms of spinodal decomposition, but the agitation makes the process much too complicated to analyse. By contrast, multicomponent thermoset resins are polymerized and cured under static conditions, hence it is rather easy to analyse the mechanism. Actually, the structure development during cure in mixtures of diglycidyl ether of bisphenol A (epoxy)/poly(ether sulfone) and epoxy/liquid nitrile rubber was investigated by light scattering and scanning electron microscopy (SEM), and revealed a reaction-induced spinodal decomposition mechanism[2,3]. A similar situation was demonstrated for the cast-polymerization of a mixture of methyl methacrylate (MMA) with poly(ethylene-*co*-vinylacetate) (EVA)[4].

In this study, we prepared PMMA/EVA alloys by polymerization-induced spinodal decomposition, observed the structure by SEM, and measured impact strength and dynamic mechanical properties. To understand the structure–properties relationship, we undertook an elastic–plastic analysis by means of the finite element method (FEM), which has been found to be a powerful aid in understanding the deformation mechanism of a polyolefinic thermoplastic elastomer[5] and rubber-toughened plastics[6,7].

EXPERIMENTAL

Materials

The MMA monomer was a commercial product, containing 5 ppm of hydroquinone monomethylether as an inhibitor. EVA was supplied by Mitsui-DuPont

* Present address: Kuraray Co. Ltd, Central Research Laboratories, Sakazu, Kurashiki, Okayama 710, Japan
† To whom correspondence should be addressed

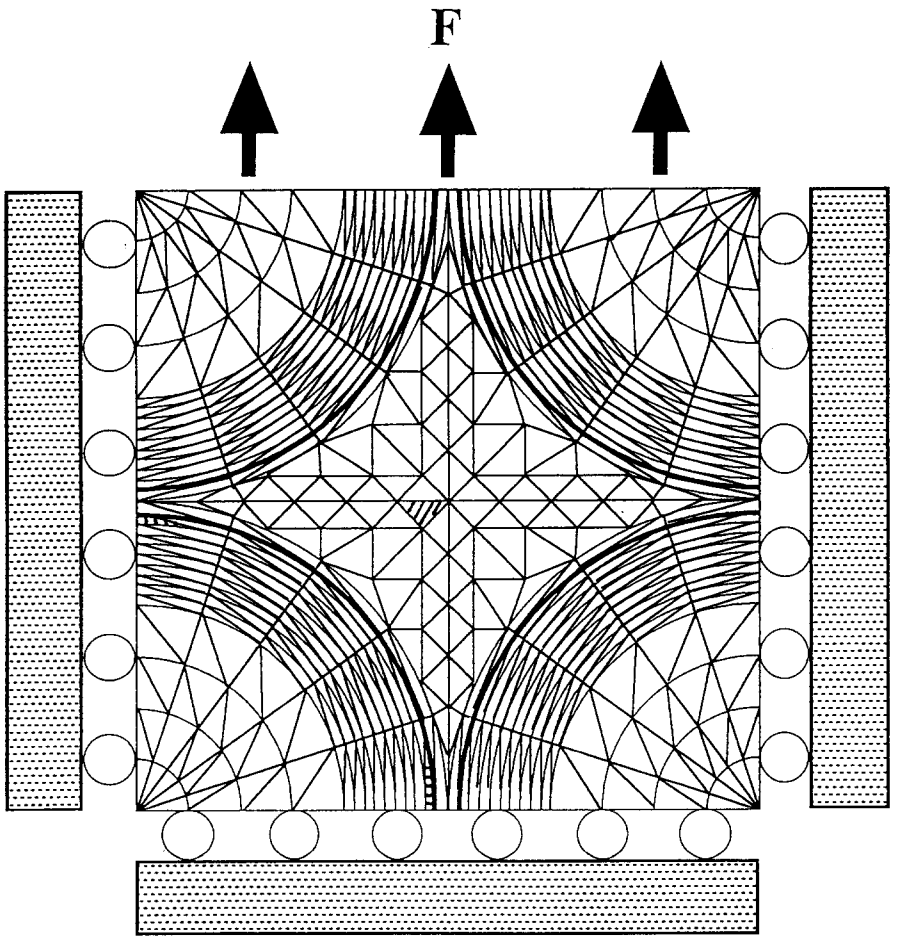

Figure 1 Two-dimensional FEM model: PMMA domains in EVA matrix

Chemical Co., Ltd (EV-45LX, 46 wt% vinylacetate content). 2,2'-Azobisisobutyronitrile (AIBN) was used as initiator. EVA was dissolved in MMA and nitrogen gas was bubbled into the solution to remove oxygen. Then the 'cast-polymerization' was performed. That is, after adding 0.25 phr of AIBN, the solution was poured into a cell comprising two glass plates with a spacer of thickness 3 mm and the cell was then closed. The polymerization was carried out quiescently in a hot chamber kept at 60°C for 20 h. To complete the reaction, the specimen was further annealed at 120°C for 1 h. EVA content was varied from 5 to 20 wt%.

Scanning electron microscopy

The two-phase morphology of the cast-polymerized specimens was observed using a Jeol T-200 scanning electron microscope, after fracturing the specimens at ambient temperature.

Impact strength test

Following the JIS-K7110 method, the notched Izod impact strength was measured for test specimens of dimensions 3 mm thick, 12.7 mm wide and 64 mm long, containing a notch of radius 0.25 mm.

The impact strength was also measured for melt blends. Neat PMMA prepared by cast-polymerization was melt-mixed with EVA at 180°C for 5 min and then injection moulded to produce the test specimen mentioned above.

Dynamic mechanical analysis

The temperature dependence of the dynamic storage modulus E' was measured by a Reospectraer (model DVE-V4, Rheology, Inc.) at 11 Hz during heating at 3°C min^{-1}. The rubbery modulus of neat EVA was measured using an RMS Mechanical Spectrometer (model 800, Rheometrics, Inc.).

FEM analysis

We constructed a two-dimensional FEM model so that four particles of PMMA were embedded in the EVA matrix as shown in *Figure 1*. By changing the radius of the particle, the volume fraction of PMMA phase was varied. Each element was assumed to have mechanical properties identical to those of the corresponding neat component polymer. That is, it was assumed that the element exhibits the same true stress–true strain curve as the component polymer. The Poisson's ratio of EVA was assumed to be 0.49 and that of PMMA equal to 0.37.

The FEM model was stretched uniaxially in the y-direction under the plane strain condition ($\varepsilon_z = 0$). The stress evolved in the x-, y- and z-directions, σ_x, σ_y and σ_z, respectively, and a shear stress τ_{xy} were calculated for each element as a function of bulk strain. Also calculated was the equivalent stress $\bar{\sigma}$, defined by:

$$\bar{\sigma} = \left\{ \frac{1}{2} [(\sigma_x - \sigma_y)^2 + (\sigma_y - \sigma_z)^2 + (\sigma_z - \sigma_x)^2 + 6\tau_{xy}^2] \right\}^{1/2} \quad (1)$$

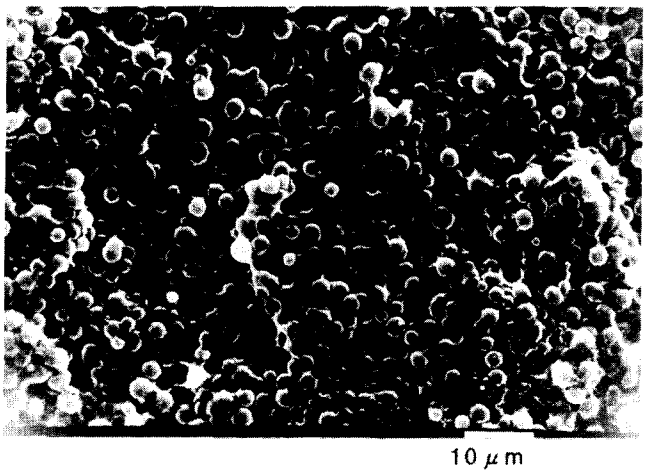

Figure 2 Scanning electron micrograph of 80/20 PMMA/EVA alloy prepared by cast-polymerization

$\bar{\sigma}$ is assumed to be a reduced tensile stress which is equivalent to the triaxial stress.

The computer program used for FEM calculations was a two-dimensional non-linear version, EPIC-IV, which can deal with elastic–plastic mechanics. Numerical calculations were carried out on a large-scale computer (Sun-3 Work Station, Sun-Microsystems, Inc.).

As described above, for elastic–plastic analyses by the FEM, it is necessary to know the true stress–true strain behaviour of the component polymers. We prepared dumb-bell specimens of the neat polymers and carried out a uniaxial tensile test. Each polymer was injection moulded into a miniature rod-type dumb-bell specimen using a Mini-Max Injection Molder (model CS-183, Custom Scientific Instruments, Inc.), as described in a previous paper[5]. Tensile testing was carried out on a Mini-Max Tensile Tester (model CS-183TE. Custom Scientific Instruments, Inc.) under a crosshead speed of 0.282 cm min^{-1}. During stretching, the diameter D of the specimen was observed by a TV video camera. From the time variations of D and the load P, the true stress σ and true strain ε' were calculated:

$$\sigma = \frac{P}{A} = \frac{4P}{\pi D^2} \tag{2}$$

$$\varepsilon' = \ln \varepsilon = \ln \frac{A_0}{A} = 2 \ln \frac{D_0}{D} \tag{3}$$

where A is the cross-sectional area of the specimen and the subscript 0 represents the unstretched state[8]. Thus the rod-type specimen provides a convenient way to estimate the variation of A with stretching by watching just D.

RESULTS AND DISCUSSION

Figure 2 shows an SEM micrograph of the 80/20 PMMA/EVA alloy prepared by cast-polymerization. A fairly regular arrangement of particles with uniform size is seen. After a rinse of the fractured specimen with carbon tetrachloride, a good solvent for EVA but not for PMMA, the same micrograph was observed. This suggests that the particles consist of PMMA and that they are embedded in a matrix of EVA. The regular two-phase structure seems to originate from spinodal decomposition[4]. It is interesting that the major component (PMMA) forms the dispersed phase, even at 80/20 composition. These situations have been discussed in more detail elsewhere[9].

The results of Izod impact tests are shown in *Figure 3*. The cast-polymerized materials show much higher impact strength than the melt blends. The 80/20 cast-polymerized material has a higher impact strength than PMMA toughened with a similar amount of conventional core–shell rubber (4.3 kg cm cm^{-1})[10]. The results suggest that cast-polymerization could be a new way forward in the design of toughened plastics.

Figure 4 shows the stress–strain curves of neat PMMA and two cast-polymerized alloys. It can be seen that the alloys have a high Young's modulus, close to that of PMMA, even though they have the two-phase structure with a rubber matrix. This situation is more clearly demonstrated by the temperature dependence of dynamic storage modulus E' in *Figure 5*. The value of E' between the glass transition temperatures of the component polymers, the so-called 'rubbery plateau modulus', is close to E' of PMMA. From the $E'(T)$ curve, one would expect the heat resistance (or heat distortion temperature (HDT)) of the alloys to be close to that of PMMA, despite their rubber matrix. However, one cannot interpret such mechanical behaviour on the basis of the classic 'series' or 'Takayanagi' model. These mechanical models are just phenomenological and too artificial to introduce morphological characteristics. FEM analysis is more promising as follows.

Figure 6 shows the stress (load F) *versus* strain curves simulated by FEM. Although the FEM model in *Figure 1* has a rubber matrix, the load F to deform the two-phase model is of the same magnitude as that required to deform PMMA. It can be seen that the experimental results in *Figure 4* are nicely depicted by the FEM analysis.

The initial slope of the stress–strain curve in *Figure 6* is the Young's modulus. Values of Young's modulus calculated by the FEM are plotted as a function of volume fraction of PMMA in *Figure 7* (open circles). These results are compared with those obtained by the series and parallel models. Basically, the parallel model is for a

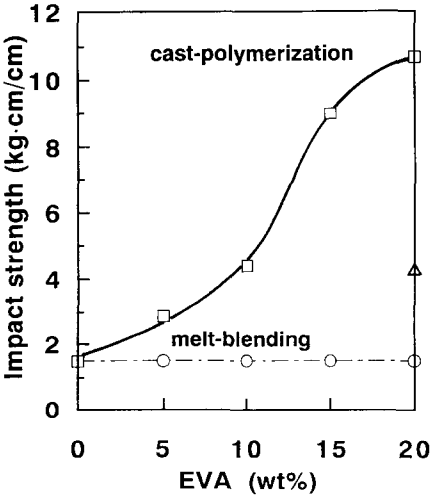

Figure 3 Notched Izod impact strength of PMMA/EVA alloys prepared by cast-polymerization and melt-blending

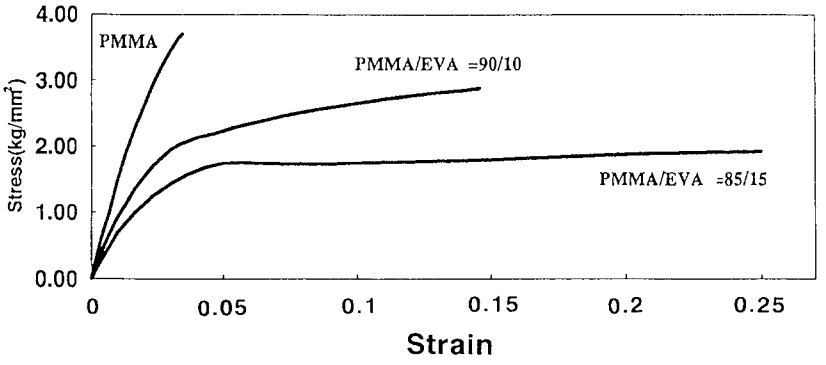

Figure 4 Stress–strain curves of PMMA, and 95/5 and 85/15 PMMA/ EVA alloys

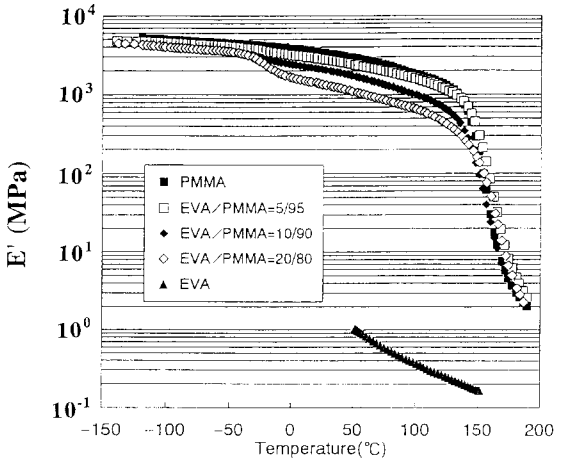

Figure 5 Temperature dependence of dynamic storage modulus E' of PMMA, EVA and PMMA/EVA alloys

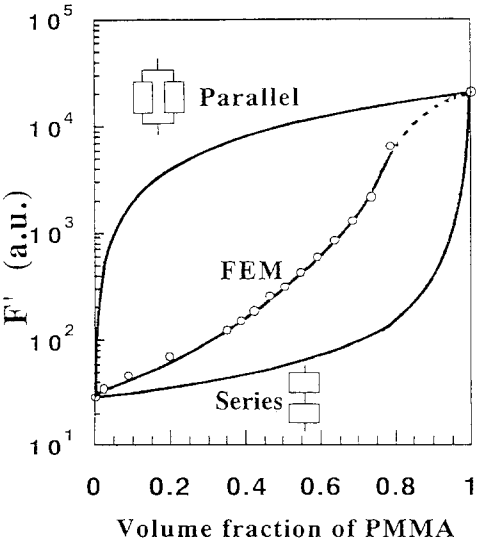

Figure 7 Modulus *versus* PMMA content

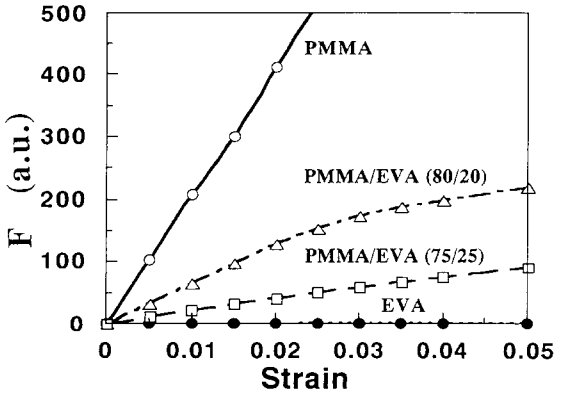

Figure 6 Load–strain curves estimated by FEM

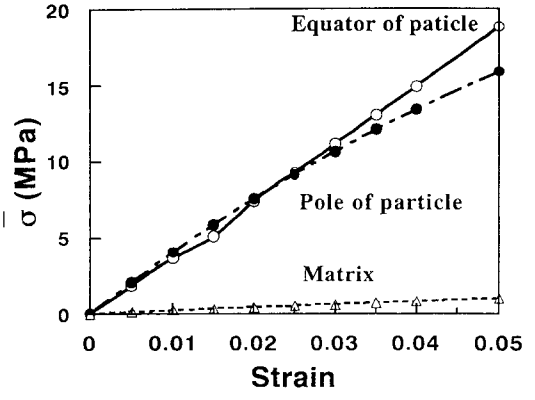

Figure 8 Equivalent stress $\bar{\sigma}$ evolved at representative FEM elements indicated in *Figure 1*, as a function of bulk strain

two-phase system of rigid matrix with soft inclusions, while the series model is for a soft matrix system. On increasing the volume fraction of PMMA, the modulus by FEM starts to deviate from that of the series model and, at high volume fraction, it is close to that of the parallel model. This apparently suggests a high level of connectivity of the PMMA phase at high volume fraction. But this is not the case, as typically demonstrated by the SEM micrograph in *Figure 2*. The question, then, is how to understand the high modulus for the rubber matrix system.

To answer the question, we calculated the equivalent stress $\bar{\sigma}$ at three representative elements in both the PMMA particle and EVA matrix, indicated as shaded elements in *Figure 1*. In *Figure 8* are shown the results for the 80/20 PMMA/EVA blend. $\bar{\sigma}$ values at equatorial and polar elements in the PMMA particle are very high, suggesting that the rigid PMMA particle is responsible

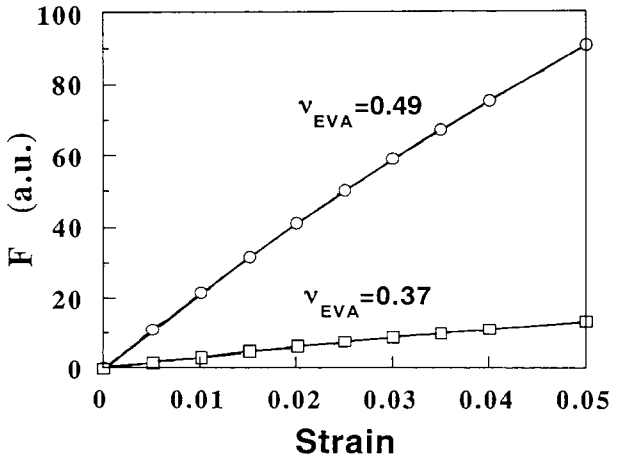

Figure 9 Load–strain curves estimated for two-phase systems with $\nu_{EVA}=0.49$ and $\nu_{EVA}=0.37$, respectively

for bulk deformation and therefore the high bulk modulus, even though it is dispersed in the rubber matrix.

The high stress level in the PMMA particle (*Figure 8*) means a finite deformation. Thus the problem to be answered is why the PMMA particle deforms during bulk deformation, i.e. why the PMMA particle deforms in the rubber matrix. Since EVA matrix has a Poisson's ratio near 0.5, it hardly changes its volume upon deformation. However, as bulk deformation causes dilation, volume strain must be induced in the PMMA particle, which has a Poisson's ratio much less than 0.5. Thus, deformation of the PMMA particle is expected to be caused by the difference in Poisson's ratio between the EVA matrix and PMMA particle. To justify this scenario, we changed the Poisson's ratio of the rubber matrix from 0.49 to 0.37 and carried out a similar FEM calculation. The result is shown in *Figure 9*. When the Poisson's ratio is small (0.37), the stress (load F) is very small and hardly depends on strain, suggesting a low bulk modulus. Thus the change in the Poisson's ratio greatly affects the rigidity of this PMMA/EVA blend.

The high impact strength of the alloys in *Figure 3* may be interpreted using the cold drawing mechanism of Kurauchi and Ohta[11] and Inoue and co-workers[12,13]. This was proposed as the toughening mechanism of plastic blends composed of a ductile polymer matrix and dispersed brittle polymer particles. In the ductile/brittle blends, the brittle particles undergo plastic deformation induced by the large compressive stress evolved by bulk deformation and impact energy is absorbed by the plastic deformation. The large compressive stress evolves when there is adequate difference in Young's modulus and Poisson's ratio between the dispersed phase (E_2, ν_2) and the matrix (E_1, ν_1) (in ductile/brittle systems, $E_2 > E_1$ and $\nu_2 < \nu_1$). The brittle polymer behaves as if it were ductile under high pressure above a certain critical value, the brittle-to-ductile transition pressure σ_c (ref. 14).

The transition pressure σ_c of PMMA at 22°C is reported[14] to be 20 MPa. In the PMMA/EVA system, such a pressure level can be attained at small strain. In *Figure 8*, one can see that the equivalent stress $\bar{\sigma}$ at both equator and pole of the PMMA particle exceeds the σ_c value at a strain of ~ 0.06. Hence the plastic deformation of PMMA particles is conceivable even in the brittle (PMMA)/rubber (EVA) system with small particle-to-particle ligament thickness, so that impact energy can be absorbed by the plastic deformation.

CONCLUSION

PMMA/EVA alloys prepared by polymerization-induced phase decomposition were shown to have a unique two-phase structure, in which particles of the major component (PMMA) were embedded in a matrix of the minor component (EVA). The alloys exhibited much higher impact strength than the melt blends and conventional PMMA toughened by a core–shell type impact modifier. The high modulus and high stress level observed in the mechanical tests, which could not be interpreted by the classic mechanical models, were analysed by FEM. The analysis elucidated that the Poisson's ratio of the EVA matrix played an important role and deformation was induced in the PMMA particle. The high impact strength was interpreted on the basis of cold drawing of PMMA particles.

REFERENCES

1 Bucknall, C. B. 'Toughened Plastics', Applied Science Publishers, London, 1977
2 Yamanaka, K. and Inoue, T. *Polymer* 1989, **30**, 662
3 Yamanaka, K., Takagi, Y. and Inoue, T. *Polymer* 1989, **30**, 1839
4 Chen, W., Kobayashi, S., Inoue, T., Ohnaga, T. and Ougizawa, T. *Polymer* 1994, **35**, 4015
5 Kikuchi, Y., Fukui, T., Okada, T. and Inoue, T. *Polym. Eng. Sci.* 1991, **31**, 1029
6 Fukui, T., Kikuchi, Y. and Inoue, T. *Polymer* 1991, **32**, 2367
7 Kojima, T., Kikuchi, Y. and Inoue, T. *Polym. Eng. Sci.* 1992, **32**, 1863
8 G'Shell, C. and Jonas, J. J. *J. Mater. Sci.* 1981, **16**, 1956
9 Ohnaga, T., Chen, W. and Inoue, T. *Polymer* 1994, **35**, 3775
10 Shah, N. *J. Mater. Sci.* 1988, **23**, 3623
11 Kurauchi, T. and Ohta, T. *J. Mater. Sci.* 1984, **19**, 1669
12 Koo, K., Inoue, T. and Miyasaka, K. *Polym. Eng. Sci.* 1985, **25**, 741
13 Angola, J. C., Fujita, Y., Sakai, T. and Inoue, T. *J. Polym. Sci. Polym. Phys. Edn* 1988, **26**, 807
14 Matsushige, K., Radclifte, S. V. and Bear, E. *J. Appl. Polym. Sci.* 1976, **20**, 1853